International Journal of Pharmaceutics 418 (2011) 199–206

Contents lists available at ScienceDirect

International Journal of Pharmaceutics

journal homepage: www.elsevier.com/locate/ijpharm

Anisotropic crystal deformation measurements determined using powder X-ray diffraction and a new *in situ* compression stage

Rahul V. Haware[a,*], Paul Kim[a], Lauren Ruffino[a], Brian Nimi[a], Catherine Fadrowsky[a], Michael Doyle[b], Stephan X.M. Boerrigter[c], Alberto Cuitino[d], Ken Morris[a]

[a] College of Pharmacy, University of Hawai'i at Hilo, 34 Rainbow Drive, Hilo, HI 96720, USA
[b] Accelrys Inc., 10188 Telesis Court, Suite 100, San Diego, CA 92121, USA
[c] SSCI, An Aptuit Company, 3065 Kent Avenue, West Lafayette, IN 47906-1076, USA
[d] Mechanical and Aerospace School of Engineering, Rutgers University, 98 Brett Road, Piscataway, NJ 08854, USA

ARTICLE INFO

Article history:
Received 21 January 2011
Received in revised form 5 June 2011
Accepted 12 June 2011
Available online 17 June 2011

Keywords:
Anisotropy
Crystal strain
Compression
Small molecular organic crystals

ABSTRACT

This report addresses the development of experimental and computational estimations of the anisotropic elastic moduli (*EM*) of single crystals to aid in the *a priori* (i.e., starting with the crystal structure) prediction of the trend as a function of the direction of applied stress. Experimentally *EM* values in the normal direction to the *X*-, *Y*- and *Z*-planes of block shaped aspirin and acetaminophen crystals were determined using data generated by the newly designed compression stage housed in our powder X-ray diffractometer. Computational estimations of *EM* were made using the applicable modules in Material Studio® 5.5. The measured *EM* values normal to the (1 0 0), (0 2 0) and (0 0 2) planes of aspirin, and (2 0 −1), (0 2 0) and (0 0 1) planes of acetaminophen crystals by both methods succeeded in detected the anisotropic behavior. However, disparity in the relative values between measured *EM* values by different techniques was observed. This may be attributed to deformation sources other than lattice compression including inelastic processes such as local failure and plasticity as well as deformation at the crystal–probe interfaces due to crystal surface roughness (asperities). The trend of the ratio of the values from the respective methods showed reasonable agreement and promise for the technique. The present approach demonstrated the suitability of the compression stage to determine and predict anisotropic *EM* of subjected small molecular organic crystals.

1. Introduction

A sound knowledge of innate pharmaceutical material properties and their response to processing stress is key to achieve an efficient manufacturing of drug product (Wang et al., 2010; Sun Changquan, 2009). This is particularly relevant in light of the ICH Q8 guideline designed to encourage the development of fundamental knowledge of every aspect of the materials and methods used in pharmaceutical development (FDA, 2006). The crystal structure of a given compound dictates both mechanical and physical properties (e.g. solubility, stability, dissolution rate and bioavailability) of pharmaceutical solids (Datta and Grant, 2004). For example, the orthorhombic Form II crystals of acetaminophen favor plastic deformation and gives better compactability than the monoclinic Form I (Joiris et al., 1998). It is also known that powders of the different polymorphic forms of various drugs like 6-chloro-2,4-dinitroaniline (Reddy et al., 2005), sulfamerazine (Sun and Grant, 2001) show very different compressibility. These varying deformation and subsequent compression properties of polymorphs may lead to potential tableting problems such as tablet capping and lamination. Modeling of these processes requires knowledge of the anisotropic response of crystalline powders under mechanical stress. Molecular crystals, by their nature introduce the necessity for an anisotropic approach to the modeling and this inherent anisotropy underlies the hypotheses in this work. The focus of this paper is on the anisotropic elastic behavior of single crystals as a first step in the study of powders, though the elastic strain has less impact than the inelastic behavior of crystals to determine compressibility (and a certain ability to regenerate molecular bonding upon the compressive forces). For the overall goal of integrating this work into the broader perspective of the NSF Engineering Research Center on Structured Organic Particulate Systems (NSF-ERC-SOPS), this is an essential component for predicting compressibility from a process development point of view. Considerations such as punch pressure, strain rate sensitivity and dwell time as well as innate material properties will become leading factors in predicting the tableting characteristics of materials. Although these broader, fundamental considerations must ultimately be addressed, here we

* Corresponding author. Tel.: +1 808 238 9795; fax: +1 808 933 2974.
E-mail address: rahulh@hawaii.edu (R.V. Haware).

0378-5173/$ – see front matter © 2011 Elsevier B.V. All rights reserved.
doi:10.1016/j.ijpharm.2011.06.021

are focusing on the first steps, i.e., what the compression stage was designed to do, namely to allow us to develop data to facilitate better predictive tools. In particular, to be able to improve force fields to not only describe equilibrium conditions, but also the behavior of organic materials under stress and, ultimately, to redesign or calibrate our force fields to perform better for this purpose. In addition data driven "constitutive" models will also be developed to correlate to other derived properties of the materials such as dissolution. However, accurate characterization of elastic properties of the materials is necessary before understanding their inelastic properties. This explains the focus of the present report.

Assessing the impact of anisotropy has been thoughtfully explored but incompletely addressed. Roberts et al. (1991) showed estimation of mechanical strength of aspirin (ASA) and primidone from their crystal structure and 3-point beam bending method. Further, anisotropic strength measurements of the single crystals of various model materials like saccharine and sucrose have been carried out by nanoindentation and microindentation techniques (Duncan-Hewitt and Weatherly, 1989a,b; Kiran et al., 2010). A major remaining gap in our understanding results from the lack of good data on the anisotropic behavior of individual crystals. The data are difficult to obtain (Duncan-Hewitt and Weatherly, 1989a,b; Kiran et al., 2010) by conventional methods and have large associated errors. This was the motivation for the development of the compression stage described in this report which exploits the expected relationship between strain and observed changes in the *d*-spacings in crystals under stress. The design of the stage also allows a traditional displacement–force determination but with greater resolution than most techniques.

The full problem of predicting the effect of the process parameters and material properties on compression process is much too broad for a single paper or project; however, we cannot hope to address the behavior of assemblies of crystallites if we do not first understand the single crystals. A single crystal may be thought of as a macroscopic model system for the crystallite but with sufficient size for us to manipulate them and perform measurements on. The aim of the present work was to develop the methodology to take the measurement of stress response to the elementary particle level (i.e., the single crystal) and to determine the anisotropic elastic moduli of small molecular organic crystals based on the combination of experimental and computational estimations of anisotropy. Aspirin and acetaminophen single crystals were used as the model compound for the validation of the methodology.

Developing the methodology is the first project in the larger NSF-ERC-SOPS goal (ERC-SOPS, 2010) to estimate deformation/compactability potential in crystalline powders from predictive methods such as explored in this report.

2. Materials

O-acetyl salicylic acid, 99% (ASA) was purchased from Alfa Aesar Johnson Matthey plc, Heysham, Lancashire, United Kingdom (Lot No. 10112030). Acetaminophen, or paracetamol (APAP) was purchased from McNeil Pharmaceuticals, Fort Washington, USA (Lot No. 0048906M504). Ethanol (96%) was purchased from Fisher Scientific, Pittsburgh, PA, USA.

3. Methods

3.1. X-ray diffractometry on single crystals during anisotropic deformation

The resulting degree of strain of single crystals under applied mechanical stress was dynamically measured by using a newly developed compression stage mounted in our powder X-ray

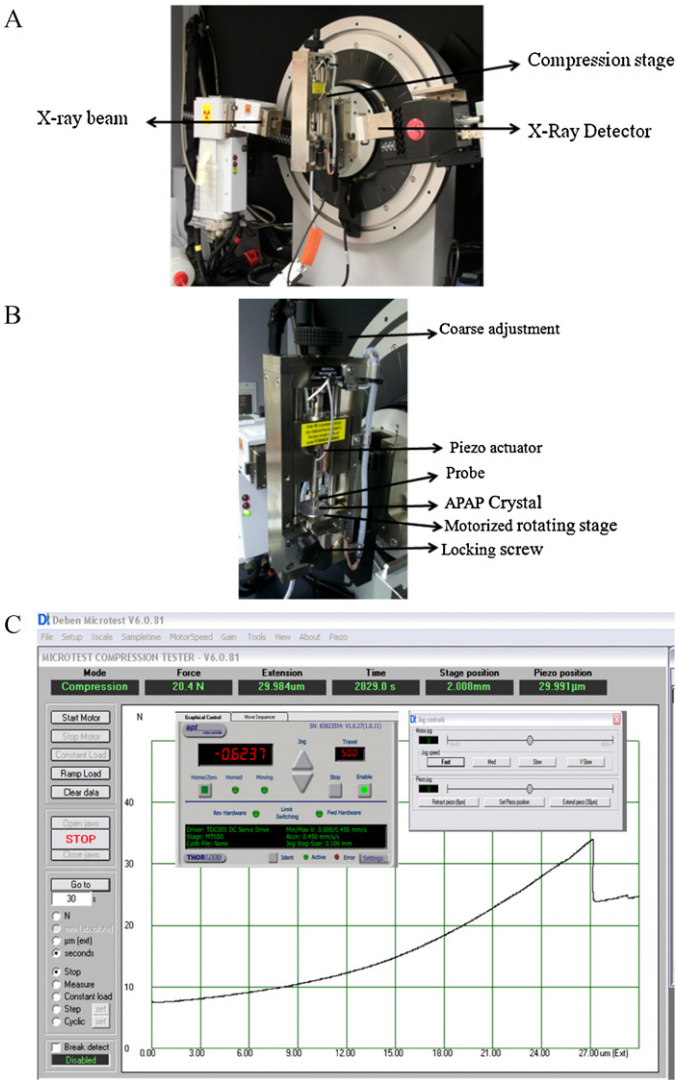

Fig. 1. (A) The compression cell housed in the Bruker D8 PXRD instrument, (B) ASA crystal compression and (C) Piezo-travel control unit software user interface.

diffraction instrument, a Bruker D8 Advance (AXS GmbH, Karlsruhe, Germany). The instrument is equipped with a vertical goniometer in the Bragg–Brentano geometry ($\theta/2\theta$). The signal is conditioned using a Göbel mirror and collected using a LYNXEYE linear detector (Fig. 1A). The open architecture of this particular instrument allows easy accommodation of the compression cell without modification. The LYNXEYE linear detector is approximately 200 times more sensitive than typical scintillation detector which accelerates data collection.

The compression stage, a Deben Microtest MT 10267 was jointly designed by the authors and the vendor (Deben UK Ltd., Suffolk, UK). It operates on the principle of mechanical compression of a subjected single crystal with variable strain rate. Fig. 1 shows the details. The stage (Fig. 1B) consists of a piezoelectric crystal attached to a probe and a crystal is held between the probe tip and the flat motorized rotation stage base. This rotation stage allows crystal rotation in 360°, about the *z*-axis which insures alignment to the desired plane. Further a coarse adjustment screw is used to increase or decrease the proximity of probe to the top potion of the crystal. Once, the desired crystal plane is located in the X-ray, the locking screw is maintain contact between the probe and the, top crystal surface, bottom crystal surface, and compression stage during the application of compression stress on the desired crystal

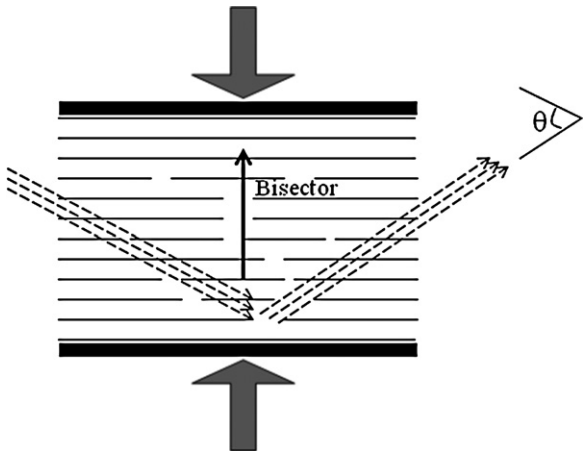

Fig. 2. Diffraction condition schematic.

plane. The probe travels to a controlled distance to exert a compression force on the single crystal (Fig. 1C). The current maximum travel is 30 μm with a resolution of 1.8 nm in single step with a maximum compression force of 50 N. The probe tips are available in different diameter sizes, e.g., 2 mm, 3.54 mm and 5 mm to match the crystal size. The stage is interfaced to the X-ray computer and fits in the X-ray instrument without interfering with the beam. Diffraction is measured in transmission, which probes the planes normal to the axis of compression (Fig. 2). The stage allows the estimation of deformation both from the analysis of the X-ray diffraction pattern (i.e., the shift in the reflection of interest) as well as from the direct control of the displacement of the probe. The applied force is the same for both methods.

3.2. Implementation of the compression stage

3.2.1. Crystal growth and shaping

ASA crystals were grown by controlled evaporation from a saturated solution in acetone at room temperature. APAP crystals were grown by solvent evaporation from a mixture of equal parts of methanol, ethanol, and acetone at room temperature (23 °C). The crystals obtained were shaped to a block shape with a micro knife or razor blade which was followed by annealing/smoothing in ethanol for 30 s at room temperature.

3.2.2. Crystal compression

Representative orientations with the *x*-, *y*- and *z*-directions parallel to the plane of the sample stage of ASA crystal (Fig. 3), i.e. (1 0 0), (0 2 0) and (0 0 2) planes respectively and APAP crystals [(2 0 −1), (0 2 0) and (0 0 1)] were selected to study changes in *d*-spacing under the applied stress in the compression stage. The compression stress was applied normal to the selected plane. Block shaped ASA crystals between approximately 2–3 mm in length and height and about 1.5 mm in width were compressed using the 3.54 mm diameter probe in order to cover entire crystal surface area at varied compression forces (i.e. from 7 to 40 N depending upon the subjected planes).

3.2.3. X-ray diffraction (XRD) under compressive stress

Changes in *d*-spacing of different ASA and APAP crystal planes under the applied stress was observed at room temperature by measuring the angle of diffraction of that particular plane. All experiments were conducted using a Cu Kα radiation point source (λ = 1.5406 Å) at an operating voltage of 40.0 kV and a current of 40.0 mA. The scanning range was dependant on the planes under study and was estimated from simulated powder patterns. The scanning rate was 0.005°/min with a step size of 0.01° for required resolution.

3.2.4. Computational modeling and analysis

ASA (CSD refcode: ACSALA01) (Kim et al., 1985) and APAP (CSD refcode: HXACAN04) (Naumov et al., 1998) crystal structures were obtained from the Cambridge Structural Database (Cambridge Crystallographic Data Centre, Cambridge, UK). The simulated PXRD patterns of these selected structures were calculated using Mercury 2.3 (Cambridge Crystallographic Data Centre, Cambridge, UK), which were used to determine respective planes in the experimentally observed reflections of the ASA and APAP single crystals.

All of the other computations were carried out using the appropriate modules/interfaces included in Materials Studio© 5.5 as described below.

3.2.4.1. Charges and optimization. The crystal structures were first subject to a forcefield based mechanical property evaluation. Using the CCDC reported crystal structures and the Density functional program DMOL3, the structures were optimized using the GGA gradient corrected PBE functional and the charges for atoms in the molecules were determined using the Mulliken population analysis method (Mulliken, 1955). The wave functions that these were based on were determined using van der Waals dispersion corrected (Grimme, 2006) non-local gradient correct density functional theory using the PBE functions (Perdew et al., 1996). The RMS values for the two structures used were: for aspirin (refcode: ACSALA01) after minimization the average atom RMS over the whole structure is 0.27700370 Å, while for the heavy atoms (non-H) it's 0.00986263 Å.

For acetaminophen (refcode: HXACAN04) after minimization the average atom RMS over the whole structure is 0.01811394 Å, while for the heavy atoms it's 0.00709671 Å.

3.2.4.2. Mechanical properties calculations. The charges were then applied to the molecules, and the two different ensembles constructed. One a conversion to P-1 of the CCDC structure and one a lattice manipulation where the *b* and *c* vectors were unchanged and a vector was converted to a new vector (2 0 −1) relative to the original lattice. Also, this structure was then converted to a primitive lattice. These cell manipulations were done using conventional crystallographic symmetry definitions and performed in using Materials Studio© 5.5 (Accelrys®, San Diego, CA, USA). Atom types were determined and assigned from the Dreiding forcefield (Mayo et al., 1990). Ewald corrections were then applied for both the long range van der Waals and electrostatic forces and the mechanical properties for the full strain tensor matrix, i.e. in the *x*-, *y*-, *z*-, *xy*-, *xz*-, *yz*-directions determined at 6 point increments for energies determined using the forcefield at convergence thresholds less than 1×10^{-4} in total energy (kcal mol^{-1}), 0.0005 in mean force (kcal mol^{-1} Å^{-1}) and 5×10^{-5} in maximum atom displacement (Å). The mechanical properties calculations used the "constant strain" approach. The process starts by removing symmetry from the system, and then generates a series of configurations. For each configuration, a number of strains are applied, resulting in a strained structure. The resulting structure is then optimized, keeping the cell parameters fixed and the energies of the complete series of strains tabulated and re-normalized to the unit cell vectors. Six strain configurations were generated between −0.003% unit strain to +0.003%. This was done for each axial direction for each primary configuration as well as for the cross tensor directions. The strain values are then used to generate the metric tensors *G*, i.e. $G = H0'[2E + I]H0$, where $H0$ are formed from the lattice vectors; I is the identity matrix and $H0'$ is the transpose of $H0$. Then the new lattice parameters were derived from *G*, these were then used to transform the cell parameters (fractional coordinates are held fixed) to the test

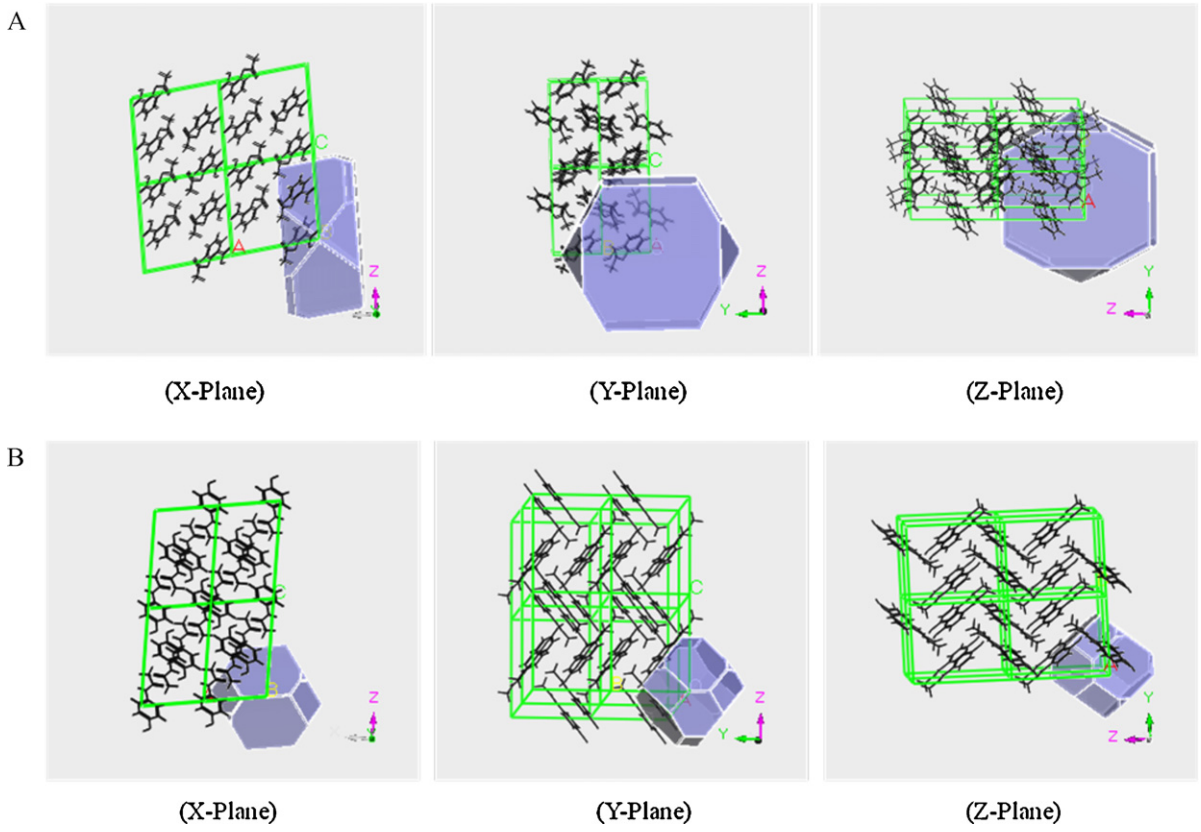

Fig. 3. Various orientations (*x*-, *y*- and *z*-planes) of (A) ASA and (B) APAP crystal subjected for the study.

states and following these steps the configuration structures were optimized using the forcefield and charges and the stress fields calculated. This approach, is similar to the work of Theodorou and Suter (1986), and uses a statics based evaluation. In this approach, it is assumed that contributions originating from changes in configurational entropy on deformation, and from the strain dependence of the vibrational frequencies ought to be negligible for the system and so it is possible to estimate the elastic stiffness coefficients from numerical estimates of $d2U/d\varepsilon_i\, d\varepsilon_j$ ($=d\sigma_i/d\varepsilon_j$). The elastic constants are determined after having constructed an energy-minimized series of structures confined by subjecting each structure to twelve deformations; three pairs in uniaxial tension/compression and three pairs involving pure shear, followed by a re-minimization to restore a state of detailed mechanical equilibrium.

3.2.5. Determination of anisotropic Young's moduli

Young's moduli were determined by measuring the deformation at the applied stresses of the crystals in different orientations. For this, the X-ray diffraction reflections of selected crystal planes compressed at various stresses were analyzed by using Eva software (Bruker-AXS-GmbH, 2002). The changes in *d*-spacing (Δd) were used as the strain values in the given direction of applied stress.

The initial value (d_0), the stress (F/A_0) and the cross-sectional area (A_0) measured by using Vernier Caliper (Reid Supply Company®, Muskegon, MI, USA) of the subjected crystal were used in combination with the slope of stress (MPa) vs. strain plot to estimate elastic Young's modulus (E) of the crystal in the given direction.

3.2.6. Macroscopic testing of the crystal strength

3.2.6.1. Young's modulus from the compression stage piezo actuator travel data. Macroscopic strain, i.e. change in the total length of the crystal with respect to its initial length, was calculated from the distance traveled by the piezo actuator to exert a required compression stress. The bulk modulus (E_S) of the respective crystal plane was calculated from the following relationship (1) (Young's-modulus):

$$E_S = \frac{FL}{A\Delta L} \quad (1)$$

where F is the compression force, A is the crystal surface area, L is the initial crystal length and ΔL is the change in length at respective compression stress.

4. Results and discussion

4.1. Implementation of the PXRD compression stage

Initially, installation qualification of the compression stage was performed after careful mounting of the stage into the PXRD. Adjustment of the stage height and calibration of goniometer angle was performed with corundum standard sample (SRM676 – NIST, 2010). A block shaped ASA crystals of approximately 3 mm as a model material was used to test the piezo throw and load cells.

ASA crystals with various orientations (Fig. 3) were used to check the ability of instrument to measure the anisotropic crystal response to the applied stress.

4.2. Anisotropic crystal strain measurement

The strain (deformation) on a single crystal generated in a compression cell housed in a PXRD should manifest directly as a change in the *d*-spacing observed in the powder X-ray diffraction pattern

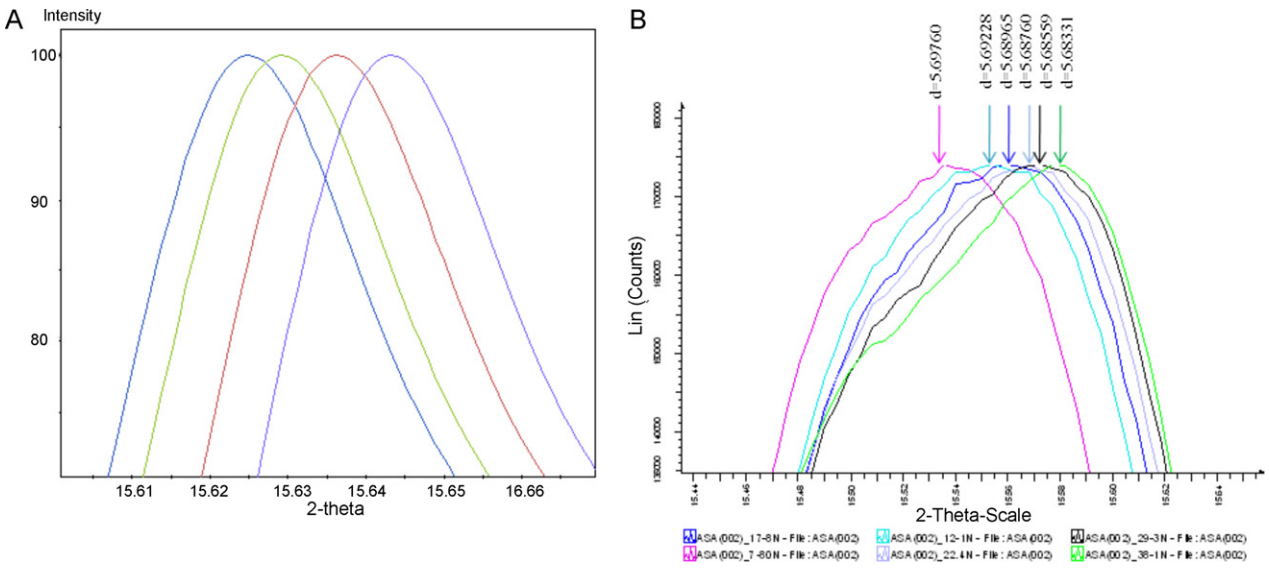

Fig. 4. *d*-Spacing shifting of ASA (0 0 2) plane under compression stress (A) simulated pattern (Materials Studio©) and (B) experimental results.

(Fig. 2). This information gathered over a range of orientations of ASA and APAP crystals was used to estimate the anisotropic strain and Young's moduli of the ASA and APAP crystal systems.

Shift in the *d*-spacing of the representative (0 0 2) plane of ASA under applied compression stress was determined computationally from the single crystal structure (Fig. 4A), which was also confirmed experimentally (Fig. 4B) in the powder X-ray diffraction pattern. The *d*-space values found decreased with increase in the compression stress.

Table 1 contains the elastic Young's moduli normal to the *x*-, *y*- and *z*-planes of ASA and APAP crystals measured from the X-ray diffraction data, stage data and their ratios. The Young's modulus values for the directions tested on the ASA and APAP crystals based on X-ray data were higher than those calculated from the stage data. A possible reason is the overall stage displacement data might reflect the rearrangement of domains in the single crystals around defects as well as some local elastic deformation. In contrast, the elastic deformation at the unit cell level (*d*-spacing) takes more force than does the "rearrangement". As a consequence, crystals at the unit cell level might be expected to show lower elastic deformation and subsequently give higher values of Young's modulus than that of determined by other techniques. As the technique requires quite large crystals it was expected (based on our experience in crystal growing) and observed that the defect density as manifest in opacity was noticeable. A similar effect very likely occurs from any slight unevenness of or asperities on, the crystals where they contact the probe. While it does not require much force to "seat" the crystal, even minor rearrangement or compression of asperities

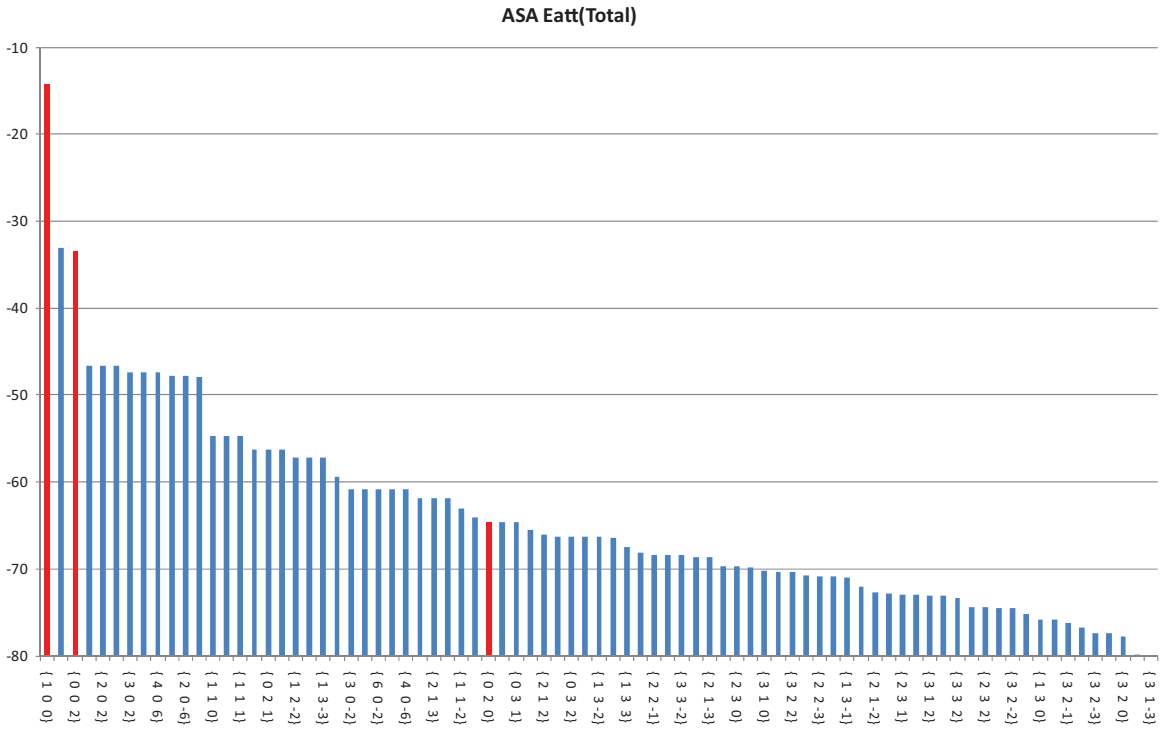

Fig. 5. Calculated attachment energies (kcal mol^{-1}) of various ASA planes.

Table 1A
Comparison of *E* values of various ASA and APAP planes obtained by different techniques.

Model material	Plane	Elastic Young's modulus (GPa)		
		X-ray*	Compression stage	Forcite MJD
ASA	(1 0 0)	1.31 (0.29)**	0.10 (0.04)**	7.82
	(0 2 0)	1.62 (0.55)**	0.40 (0.26)**	11.09
	(0 0 2)	4.61 (0.81)**	0.19 (0.07)**	19.34
APAP	(2 0 −1)	2.96 (0.65)**	0.28 (0.17)**	1.88
	(0 2 0)	1.09 (0.04)**	0.11 (0.01)	0.354
	(0 0 1)	2.95 (0.74)	0.21 (0.137)	0.764

* Average of three measurements carried on three individual crystals.
** Std. deviation.

Table 1B
Normalized YM values to plane having lowest value for ASA and APAP single crystals.

Model material	Normalized Young's moduli			
	Plane	X-ray	Stage	Forcite MJD
ASA	(1 0 0)	1.00	1.00	1.00
	(0 2 0)	1.24	4.00	1.42
	(0 0 2)	3.52	1.90	2.47
APAP	(2 0 −1)	2.72	2.55	5.31
	(0 2 0)	1.00	1.00	1.00
	(0 0 1)	2.71	1.91	2.16

would show up as displacement or strain. Every attempt was made to achieve molecularly smooth surfaces however this is not a trivial task and some faces lend themselves to cleaving more cleanly than others. Further, Young's moduli determined as a function of direction (X-ray and stage data) showed some disparity with that from literature values (Duncan-Hewitt and Weatherly, 1989a,b; Kiran et al., 2010).

Fig. 5 shows the attachment energy associated with various possible ASA crystal planes. Out of the subjected ASA planes, (0 2 0) plane showed the highest attachment energy, while (1 0 0) plane showed the lowest attachment energy. High attachment energy is typically associated with smaller *d*-spacing (Osborn et al., 1999). These directions logically exhibit high resistance to compression and subsequently show higher elastic Young's moduli. The Young's modulus value on the (0 2 0) plane obtained from the stage data was found to be higher than that of the (1 0 0) and (0 0 2) planes. However, this was not observed with the Young's modulus obtained from the X-ray data.

The ultimate goal of the continued research on this topic is of course to develop a predictive method for estimating relative crystal strength for use in "down-stream" models (e.g., FEM) of powder compaction and others. The approach explored here used modules in Materials Studio® to estimate the mechanical properties of interest. As discussed in the methods section, the reference crystal structures obtained from the CSD were first assigned point charges fitted to the electrostatic potential and then the properties were calculated using the Forcite module controlling the variables for the purpose. The challenge was to calculate the moduli for planes not assigned as *x*, *y*, or *z*, which was accomplished by re-defining the lattice (first converting to the P1 space group) to put the plane in question in the proper orientation (e.g., (2 0 −1) for APAP was re-defined as *x*). This as well as other modifications detailed above for the basis for the initial methodology for predicting the anisotropy (Fig. 6).

The results in Table 1 and Fig. 7 show several interesting trends. First the trend in *EM* for ASA determined by X-ray agrees with the calculation, while that from the direct strain measured by the stage does not agree for the *y*-direction [(0 2 0) plane)]. The magnitudes of the X-ray and Forcite determined values are different in absolute value yet closer than those determined by the strain from the piezo-actuator displacement. This makes sense as the both the X-ray and Forcite determined values are focused on deformation at the unit cell level. Examination of the crystal structure and intuition might lead to thinking the normal to (0 2 0) should be stiffer than the *x*- or *z*-directions, however, the ability of the system to yield locally normal to the (0 2 0) shows up in the energetics calculation. Even if local yield occurs in the experiment it would likely not be visible as unit cell level deformation but would appear as strain. This could be

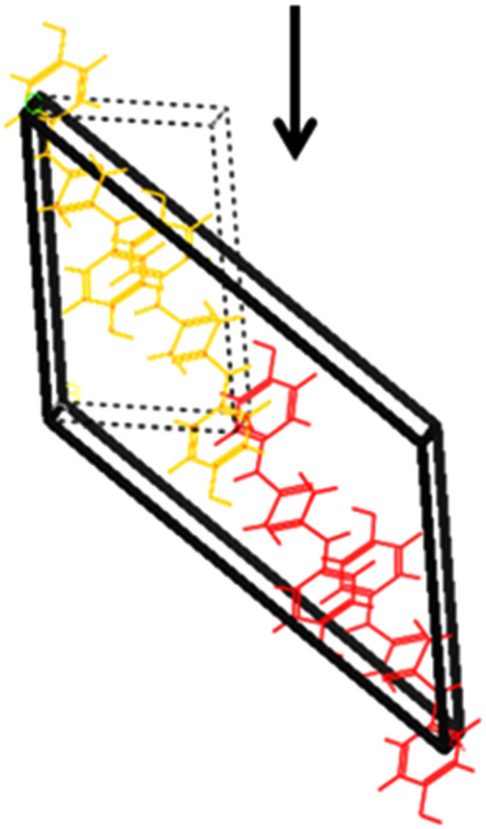

Fig. 6. Redefined lattice for APAP crystal looking down on *y*-axis show the preservation of molecular positions, while allowing the computational application of stress on the (2 0 −1) plane of an interest. Arrow indicates direction of the application of compression stress.

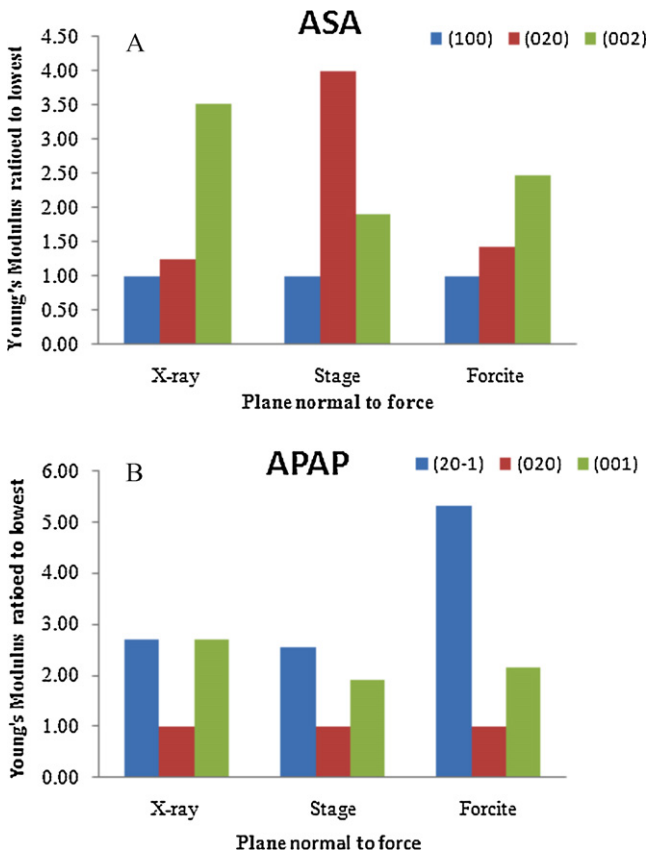

Fig. 7. Comparison of YM normalized to plane having lowest value for (A) ASA and (B) APAP single crystals. Values used in normalization are average value of three measurements carried on three individual crystals.

a way of differentiating between plastic vs. elastic deformation too subtle to show up in a simple stress–strain study, for example. The relatively larger value for the *z*-direction (i.e. normal to the (0 0 1) plane) by X-ray and Forcite analysis may be explained by examination of the structure which shows that although the largest cell dimension, deformation normal to that plane requires disruption of the strongest hydrogen bonding direction in the lattice. The significance of identifying this non-intuitive type of difference is a benefit of the multi-technique approach and the significance will be the subject of continued investigation.

The data from APAP are less distinct between techniques in that they all show the same trend and are in rank agreement with the Forcite mechanical properties estimation. However, the ratio of the magnitudes of Young's moduli is quite different. It is clear from examination of the crystal structure and computation that the (0 2 0) normal should give the lowest modulus as it does with all methods, however, the relative magnitude in the *x*- and *y*-directions is less clear. Given the standard deviations in the X-ray measurements, it is possible that further study will show the same trend.

Now that the stage and methodology are in place, much more data will be collected to populate datasets to refine the force field and develop training sets for other semi-empirical relationships.

5. Conclusions

The design, fabrication, implementation and testing of a compression stage that is mounted in an X-ray diffractometer to monitor changes in *d*-spacing in a single crystal was accomplished. The preliminary studies performed on single crystals of aspirin and acetaminophen showed the system detected anisotropy with sufficient sensitivity for the intended purpose of estimating Young's moduli in the selected directions for the single crystals. In addition, the distinct differences exhibited between X-ray determined unit cell level deformation and "macroscopic" (stress–strain) techniques gives rise to many questions, however the difference in the length scales of interrogation may allow closer evaluation of deformation mechanisms and crystal quality (i.e., defect density, etc.) and succeed in explaining at least one non-intuitive trend. Possible explanations for the disparity include asperities at the interfaces between the crystal and the probe which rearrange with stress showing up as displacement in the piezo actuator travel but not in *d*-spacing as *d*-spacing results depend solely on changes in diffraction from the desired planes, and/or local yield along deformable directions in the lattice.

Importantly for the study, examinations of the single crystal structures were useful in establishing the reasonableness of the hypothesis that changes in *d*-spacing are proportional to fundamental strain. Further, that some of the disparities observed between the Young's moduli from the experimental and computational estimates may be logical from examination of the crystal structure. Eventually the goal of the overall project is to use data generated by the methodology to refine predictive methods to allow *a priori* estimation of the trends in mechanical properties for single crystals with the intent of treating powders of crystallites as typically found in pharmaceutical manufacturing and development processes. The predictive methods used for this early stage of the work provided are a good match in establishing trends in Young's moduli and are being refined to lead to modified force field parameters and other improvements. While the predictions are encouraging it is clear that a significant amount of data will be needed to complete the training/refining of our predictive methods. As these data are generated they will be used to modeled/calibrated to improve the agreement for relevant pharmaceutical systems.

Acknowledgments

The authors are gratefully acknowledged the help and support of Gary Edwards at Deben UK Limited, UK and Holger Cordes at Bruker Corporation, USA for help in designing compression stage and PXRD respectively. We are also thankful to Alexander Laurich of the Institute for Astronomy at the University of Hawaii at Hilo for helping in the modification, installation and qualification of compression stage in PXRD.

References

Bruker-AXS-GmbH, 2002. Point, Click and Analyse Your XRD Data-Diffractplus EVA. http://www.bruker-axs.de/uploads/tx_linkselector/DIFFRACplusEVA_Spec_Sheet_S88-E01001.pdf.12/08/10.
Datta, S., Grant, D.J., 2004. Crystal structures of drugs: advances in determination, prediction and engineering. Nat. Rev. Drug Discov. 3, 42–57.
Duncan-Hewitt, W.C., Weatherly, G.C., 1989a. Evaluating the deformation kinetics of sucrose crystals using microindentation techniques. Pharm. Res. 6, 1060–1066.
Duncan-Hewitt, W.C., Weatherly, G.C., 1989b. Evaluating the hardness, Young's modulus, and fracture toughness of some pharmaceutical crystals using microindentation techniques. J. Mater. Sci. 8, 1350–1352.
ERC-SOPS, 2010. Engineering Research Centre for Structured Organic Particulate Systems. http://www.ercforsops.org/.12/15/10.
FDA, 2006. Guidance for Industry: Q8 Pharmaceutical Development. http://www.fda.gov/downloads/RegulatoryInformation/Guidances/ucm128029.pdf (12/27/10).
Grimme, S., 2006. Semiempirical GGA-type density functional constructed with a long-range dispersion correction. J. Comput. Chem. 27, 1787–1799.
Joiris, E., Di Martino, P., Berneron, C., Guyot-Hermann, A.M., Guyot, J.C., 1998. Compression behavior of orthorhombic paracetamol. Pharm. Res. 15, 1122–1130.
Kim, Y., Machida, K., Taga, T., Osaki, K., 1985. Structure redetermination and packing analysis of aspirin crystal. Chem. Pharm. Bull. 33, 2641–2647.
Kiran, M.S.R.N., Varughese, S., Reddy, C.M., Ramamurty, U., Desiraju, G.R., 2010. Mechanical anisotropy in crystalline saccharin: nanoindentation studies. Cryst. Growth Des. 10, 4650–4655.

Mayo, S.L., Olafson, B.D., Goddard, W.A.I., 1990. Driding: a generic forcefield. J. Phys. Chem. 94, 8897–8909.
Mulliken, R.S., 1955. Electronic population analysis on LCAO-MO [linear combination of atomic orbital–molecular orbital] molecular wave functions. I. J. Chem. Phys. 23, 1833–1840.
Naumov, D.Y., Vasilchenko, M.A., Howard, J.A.K., 1998. The monoclinic form of acetaminophen at 150 K. Acta Crystallogr., Sect. C: Cryst. Struct. Commun. C 54, 653–655.
Osborn, J.C., York, P., Rowe, R.C., Roberts, R.J., 1999. Prediction of slip planes in molecular crystals by molecular modeling. In: Int. Symp. Ind. Cryst. 14th FIELD , pp. 1166–1174.
Perdew, J.P., Burke, K., Ernzerhof, M., 1996. Generalized gradient approximation made simple. Phys. Rev. Lett. 77, 3865–3868.
Reddy, C.M., Basavoju, S., Desiraju, G.R., 2005. Sorting of polymorphs based on mechanical properties. Trimorphs of 6-chloro-2,4-dinitroaniline. Chem. Commun., 2439–2441.
Roberts, R.J., Rowe, R.C., York, P., 1991. The relationship between Young's modulus of elasticity of organic solids and their molecular structure. Powder Technol. 65, 139–146.
Sun, C., Grant, D.J.W., 2001. Influence of crystal structure on the tableting properties of sulfamerazine polymorphs. Pharm. Res. 18, 274–280.
Sun Changquan, C., 2009. Materials science tetrahedron—a useful tool for pharmaceutical research and development. J. Pharm. Sci. 98, 1671–1687.
Theodorou, D.N., Suter, U.W., 1986. Atomistic modeling of mechanical properties of polymeric glasses. Macromolecules 19, 139–154.
Wang, J., Davidovich, M., Desai, D., Bu, D., Hussain, M., Morris, K., 2010. Solid-state interactions of a drug substance and excipients and their impact on tablet dissolution: a thermal–mechanical facilitated process-induced transformation or PIT. J. Pharm. Sci. 99, 3849–3862, https://www-s.nist.gov/srmors/view_detail.cfm?srm=676 (01/19/10).
Young's-modulus. http://en.wikipedia.org/wiki/Young%27s_modulus (12/08/10).